Hindawi
Mathematical Problems in Engineering
Volume 2019, Article ID 7501524, 10 pages
https://doi.org/10.1155/2019/7501524

Research Article

Improved Performance Prediction of Marine Propeller: Numerical Investigation and Experimental Verification

Yue Tan,[1] Jing Li,[2] Yuan Li,[2] and Chunbao Liu [2]

[1]*School of Mechanical Engineering, Shenyang Institute of Engineering, Shenyang 100136, China*
[2]*School of Mechanical Science and Aerospace Engineering, Jilin University, Changchun 130012, China*

Correspondence should be addressed to Chunbao Liu; liuchunbao@jlu.edu.cn

Received 4 October 2018; Revised 28 January 2019; Accepted 2 April 2019; Published 18 April 2019

Academic Editor: Jan Koci

An approach was presented to improve the performance prediction of marine propeller through computational fluid dynamics (CFD). After a series of computations were conducted, it was found that the passage in the former study was too narrow, resulting in the unnecessary radial outer boundary effects. Hence, in this study, a fatter passage model was employed to avoid unnecessary effects, in which the diameter was the same as the length from the propeller to the downstream outlet and the diameter was larger than the previous study. The diameter and length of the passage were 5D and 8D, respectively. The propeller DTMB P5168 was used to evaluate the fat passage model. During simulation, the classical RANS model (standard k-ε) and the Multiple Reference Frame (MRF) approach were employed after accounting for other factors. The computational performance results were compared with the experimental values, which showed that they were in good agreement. The maximum errors of K_t and K_q were less than 5% and 3% on different advance coefficients J except 1.51, respectively, and that of η was less than 2.62%. Hence the new model obtains more accurate performance prediction compared with published literatures. The circumferentially averaged velocity components were also compared with the experimental results. The axial and tangential velocity components were also in good agreement with the experimental data. Specifically, the errors of the axial and tangential velocity components were less than 3%, when the r/R was not less than 3.4. When the J value was larger, the variation trends of radial velocity were consistent with the experimental data. In conclusion, the fat passage model proposed here was applicable to obtain the highly accurate predicted results.

1. Introduction

The performance of propellers is of significant importance as it affects the overall performance of the machinery. Nowadays, computational fluid dynamics (CFD) is extensively used for the design purposes, allowing experimental tests to be performed only in the final stages of the project. With reference to propeller applications, CFD simulations can be used to predict the flow around propellers and their performances. Therefore, with the continuous improvement of propeller's performance prediction, numerical research rather than experiment can ultimately be achieved in a cheaper and faster way.

In recent years, researchers had used different computational domain and turbulence models to conduct studies of the propellers, which validated the feasibility of numerical methods to some extent in comparison with the experimental data. Paterson et al. [1] demonstrated the capability of computational domain with a single blade passage to simulate practical ship hydrodynamics. PTakayuki et al. [2] conducted numerical simulations of the full propeller geometry structure with five blades by a RANS CFD code, and they concluded that RANS approach was applicable to the propeller flow simulation under cavitation and noncavitation conditions. In the subsequent study, a multitude of researchers investigated the performances of propeller by the whole computational domain, and the results of the computation were in good agreement with the experimental data [3–6]. Since the flow around a marine propeller working in a homogeneous uniform flow was periodic, with respect to the blades, a sea of numerical predictions was performed considering only one blade passage (see, for example, Sun [7] and Morgut et al. [8, 9]). With respect to the turbulence models, many models, if not most, had been implemented

to calculate the performance of a marine propeller. Zhao [10] employed Spalart-Allmaras turbulence model and the whole blades passage to simulate the flow around propeller. The computational results did not deviate largely from the experiment, and the details of the tip velocities were captured. Wang et al. [11] carried out the computational analysis of marine propeller performance with the whole blades passage by using the SST k-ω turbulence model and the transition-sensitive turbulence model (TSM). It was found that the applied transition-sensitive turbulence model was better able to resolve blade surface stresses, flow separation, and tip vortex originations. Morgut et al. [8] predicted the flow around marine propellers by the SST (Shear Stress Transport) two-equation turbulence model. Dubbioso et al. [12] analyzed the propeller bearing loads with the whole blades behind skeg passage by means of URANS simulations. They also used velocity and vorticity fields to describe the pressure distribution on different representative blade sections and the downstream wake at a wide range of incidence angles (10–50°) by means of a dynamic overlapping grid technique [13, 14].

Some more advanced but computationally demanding models were also discussed. Yu et al. [15] conducted the simulation of unsteady cavitation flow around a highly skewed propeller with all the blades passage by an explicit LES approach with k-μ subgrid model. Mascio et al. applied detached-eddy simulation (DES) model and power spectral density (PSD) to analyze the different behaviors of the wake instabilities for the flow past a marine propeller in oblique flow operating in pure axisymmetric flow and in drift with angle of 20°. They found that the role of the secondary vorticity as well as the hub vortex seemed to be crucial in the former, and the increasing interaction of the main vorticity confined in the tip vortex was the main course in the latter [16].Chase et al. [17] evaluated RANS, DES, delayed detached-eddy simulation (DDES), and no turbulence model (NTM) by the overset grid system and a whole blades passage to obtain the open water characteristics and the vertical structure of the generic submarine propeller INSEAN E1619.

It was noteworthy that the whole blades passage could acquire the flow more directly than a single blade passage, because the flow got from a single passage had to duplicate roughly to form the whole flow filed. The computational domain was subdivided into *Rotating* and *Fixed* parts. Because the passage in the former study was too narrow and potentially affected the results, in which a relative small diameter was chosen. In this study, a fat passage model was employed in which the diameter was the same as the length from the propeller to the downstream outlet, and the diameter was larger than the previous study. The diameter and the length of passage were 5D and 8D, respectively. Hence, the computational domain was called the fat passage model.

The propeller DTMB P5168 was used to evaluate the fat passage model. Meanwhile, the standard k-ε model, as a classical RANS model, was historically the most widely used turbulence model in industrial CFD [18]. During simulation, the classical RANS model (standard k-ε) and the Multiple Reference Frame (MRF) approach were employed after accounting for other factors. By using the fat passage model, the study aimed to advance prediction ability of performances of the marine propellers in steady flow phenomena. The simulation results were verified by experimental data. Moreover, the performance prediction was improved striking. It should be noted that accurate prediction was of significant value. Once the accuracy was good enough, the propellers could be designed by computational simulations to a large extent.

2. Numerical Simulation

2.1. Governed Equations. The standard k-ε model is a model based on model transport equations for the turbulence kinetic energy (k) and its dissipation rate (ε) [19]. The model transport equation for k is derived from the exact equation, while the model transport equation for ε was obtained using physical reasoning and bears little resemblance to its mathematically exact counterpart.

In the derivation of the k-ε model, the assumption is that the flow is fully turbulent, and the effects of molecular viscosity are negligible. The standard k-ε model is therefore valid only for fully turbulent flows.

The turbulence kinetic energy, k, and its rate of dissipation, ε, are obtained from the following transport equations:

$$\frac{\partial}{\partial \mathrm{t}}(\rho k) + \frac{\partial}{\partial x_i}(\rho k u_i) = \frac{\partial}{\partial x_j}\left[\left(\mu + \frac{\mu_t}{\sigma_k}\right)\frac{\partial \mathrm{k}}{\partial x_j}\right] + \mathrm{G_k} + \mathrm{G_b} - \rho\varepsilon - \mathrm{Y}_M + \mathrm{S}_k \tag{1}$$

and

$$\frac{\partial}{\partial \mathrm{t}}(\rho\varepsilon) + \frac{\partial}{\partial x_i}(\rho\varepsilon u_i) = \frac{\partial}{\partial x_j}\left[\left(\mu + \frac{\mu_t}{\sigma_\varepsilon}\right)\frac{\partial \varepsilon}{\partial x_j}\right] + \mathrm{C}_{1\varepsilon}\frac{\varepsilon}{k} + \left(\mathrm{G_k} + \mathrm{C}_{3\varepsilon}\mathrm{G_b}\right) - \mathrm{C}_{2\varepsilon}\rho\frac{\varepsilon^2}{k} - \mathrm{Y}_M + \mathrm{S}_\varepsilon \tag{2}$$

In these equations, G_k represents the generation of turbulence kinetic energy due to the mean velocity gradients, G_b is the generation of turbulence kinetic energy due to buoyancy, $\mathrm{Y_M}$ represents the contribution of the fluctuating dilatation in compressible turbulence to the overall dissipation rate. The $\mathrm{C}_{1\varepsilon}$, $\mathrm{C}_{2\varepsilon}$, and $\mathrm{C}_{3\varepsilon}$ are constants. The σ_k and σ_ε are the turbulent Prandtl numbers for k and ε, respectively. The S_k and S_ε are user-defined source terms.

The turbulent (or eddy) viscosity, μ_t, is computed by combining k and ε as follows:

$$\mu_t = \rho C_\mu \frac{k^2}{\varepsilon} \tag{3}$$

where C_μ is a constant.

2.2. Computational Setup and Solution. As shown in Figure 1(a), the model used in the experiment and simulation was DTMB P5168 with a diameter of 0.4027m, which is a five-blade propeller with controllable pitch and highly skewed

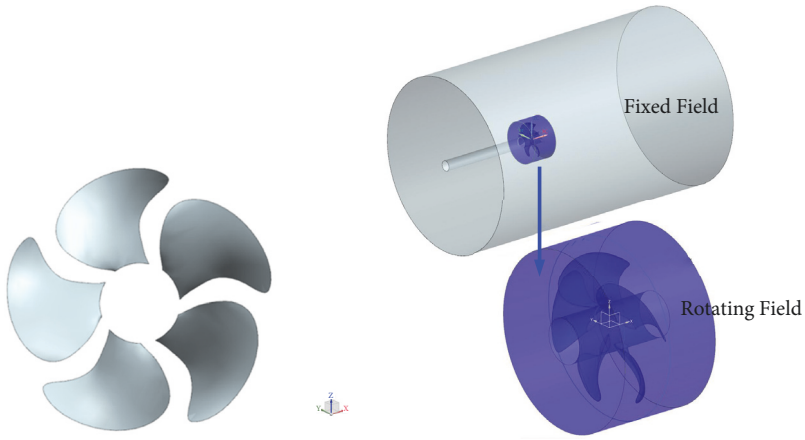

Figure 1: (a) DTMB P5168 model; (b) computational domain.

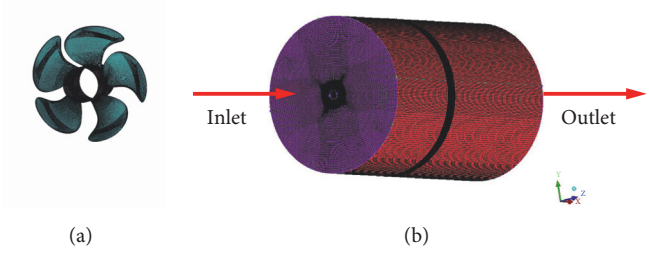

Figure 2: (a) DTMB P5168 blade surface meshes; (b) global grids.

propeller designed in David Taylor Model Basin (DTMB). In the course of experiment, the tip vortex cavitation inception and the near-tip velocity distribution in the uniform inflow were detailed investigated, which can provide some data reference for numerical simulation. The measurements, which were taken at the David Taylor 36-inch Variable Pressure Water Tunnel designed by Chesnakas and Jessup [20], were employed to verify the numerical simulation in this paper.

Taking the propeller blade as the origin and the flow direction of the liquid as the positive direction of the x-axis, a region of cylinder with a diameter of $5D$ and a length of $8D$ was designed as a computational domain. The domain extended $3D$ upstream and $5D$ downstream of the propeller. The whole cylinder domain of calculation is divided into two independently computed regions: the rotating field and fixed field. The rotating field is a small cylinder region with a diameter of $1.2\ D$ and a length of $0.7\ D$. The Multiple Reference Frame (*MRF*) approach was used to transfer the flow information through the interface of two parts.

Figure 2(a) showed the blade surface meshes of the propeller. The whole grids were showed in Figure 2(b). The grid of the whole region is a hexahedral mesh generated by *ANSYS-ICEM CFD*. It can be seen from the data in Table 1 that related settings in simulation are given.

The propeller motion can be divided into rotating motion around its own axis and moving along the axis direction, which can be replaced by n and v, respectively. In addition, the interaction force between the propeller and the water is used to drive the ship's motion, and the velocity between the two is the same in the opposite direction. The velocity of flow can be used instead of the velocity of the propeller. In order to synthetically consider the two kinds of motion of propeller, the advance coefficient is used to replace the motion state of propeller. The advance coefficient was defined as

$$J = \frac{V}{nD} \tag{4}$$

where n (r/s) was the rotational speed of the propeller and the rotational speed of the propeller n was directly set as 20 r/s, V (m/s) was the incoming flow velocity, and D (m) was the diameter of the propeller disk.

By applying the fluid velocity to the propeller instead of the forward propulsion velocity, six groups of different advance coefficients (J=0.9, 0.98, 1.1, 1.2, 1.27, and 1.51) were numerically simulated.

3. Comparison between Experiment and Calculation

The notation used throughout the paper was as follows. Thrust T was the axial component of force and torque Q was the axial component of the moment. Nondimensional thrust

Table 1: Related settings in simulation.

Numerical method	Settings/Value
Inlet and the radial outer boundary setting	A free-stream velocity components turbulence intensity: 1%
Outlet setting	Pressure-outlet static pressure: 0 Pa
all solid surfaces setting	No Slip boundary condition
Calculation model	The standard k-ε model
Calculation scheme	SIMPLEC
Momentum	Second-order backward discretization
pressure	a body force weighted

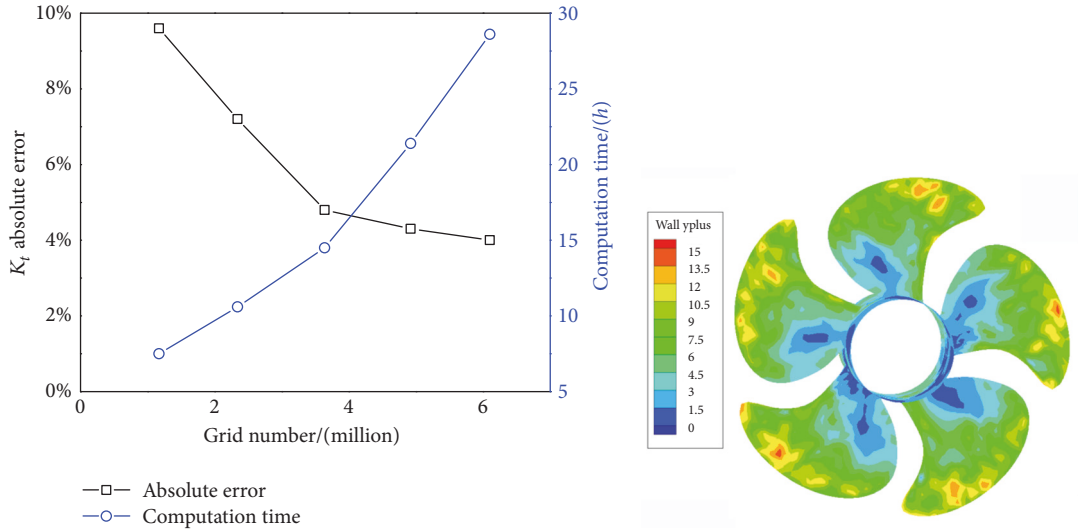

(a) (b)

Figure 3: (a) Grid independence study; (b) the y+ distribution on the blade surface.

coefficient K_t, torque coefficient K_q, and propeller efficiency η were given by

$$K_t = \frac{T}{\rho n^2 D^4},$$
$$K_q = \frac{Q}{\rho n^2 D^5}, \quad (5)$$
$$\eta = \frac{J}{2\pi} \cdot \frac{Kt}{Kq}$$

where n (r/s) was the rotational speed of the given propeller, D (m) was the diameter of the propeller, and ρ (kg/m^3) was the density of the fluid.

The relative percentage errors $\triangle K_t$, $\triangle K_q$, and $\triangle K_\eta$ listed in the pictures were defined as

$$\triangle Kt\,(\%) = \frac{Kt_{CFD} - Kt_{EXP}}{Kt_{EXP}} \cdot 100\% \quad (6)$$

$$\triangle Kq\,(\%) = \frac{Kq_{CFD} - Kq_{EXP}}{Kq_{EXP}} \cdot 100\% \quad (7)$$

$$\triangle K\eta\,(\%) = \frac{K\eta_{CFD} - K\eta_{EXP}}{K\eta_{EXP}} \cdot 100\% \quad (8)$$

Before the CFD calculation, a grid independence study at J=1.27 was carried out as shown in Figure 3 to balance computation time and accuracy. The calculation results were considered to have converged when all normalized residuals in mass and momentum conservation equations were less than 10^{-3}, and the number of iterations reached 5000. Finally, the total grid number was 3.6 million, which included 1.4 million of the rotating part and 2.2 million of the fixed part. In addition, there were 0.1 million and 0.68 million gird cells in the blade part and hub part, respectively. Figure 4 showed the ability of the RANS model to accurately analyze the boundary layer. It was shown that main values of y+ on the blade surface were less than 12, indicating that the grid resolution could well solve the Navier-Stokes equations in the near-wall regions [21].

Figures 4–6 are the curves of K_t, K_q, and η changing with J in experiments and simulations, respectively, where it was seen that the simulation results were in good agreement with the experimental data. As shown in Figure 7, except for the case of J=1.51, on different advance coefficients J, the errors of K_t and K_q were less than 5% and 3%, respectively. However, no matter what value J took, the error of η was less than 2.62%. In Paterson et al.'s work [1], the errors of K_t and K_q were in the range of 1.0%~2.9% and 1.3%~2.8% at the advance coefficient

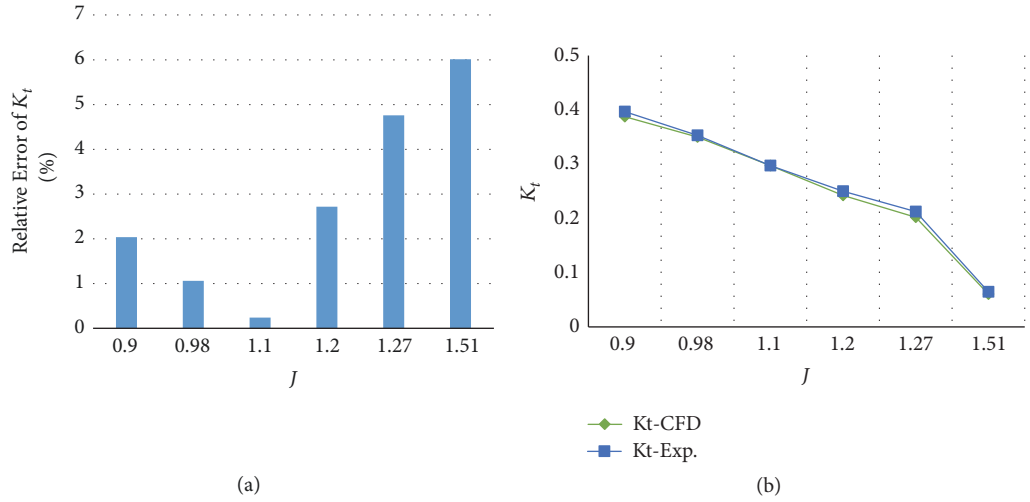

FIGURE 4: (a) A relative error diagram of simulated results of dimensionless thrust coefficient K_t; (b) hydrodynamic performance prediction and test curve of K_t.

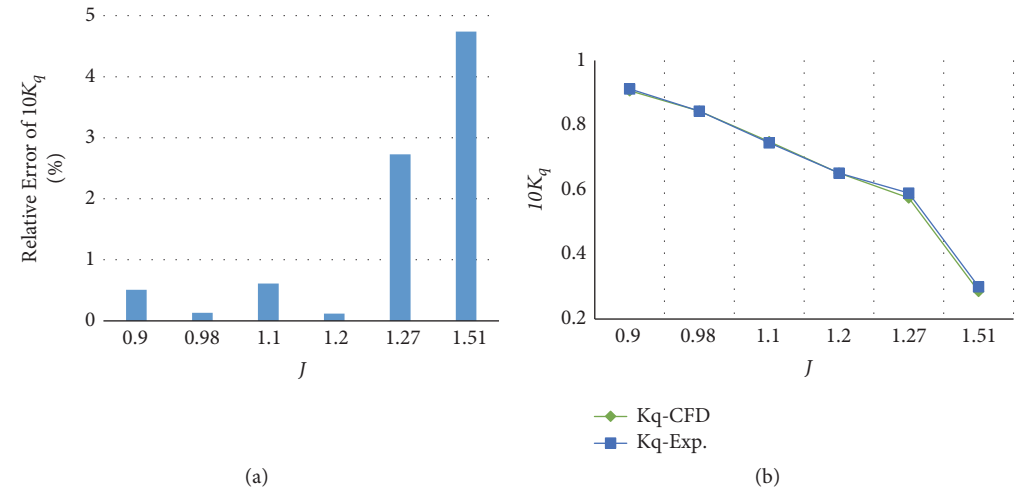

FIGURE 5: (a) A relative error diagram of simulated results of torque coefficient K_q; (b) hydrodynamic performance prediction and test curve of K_q.

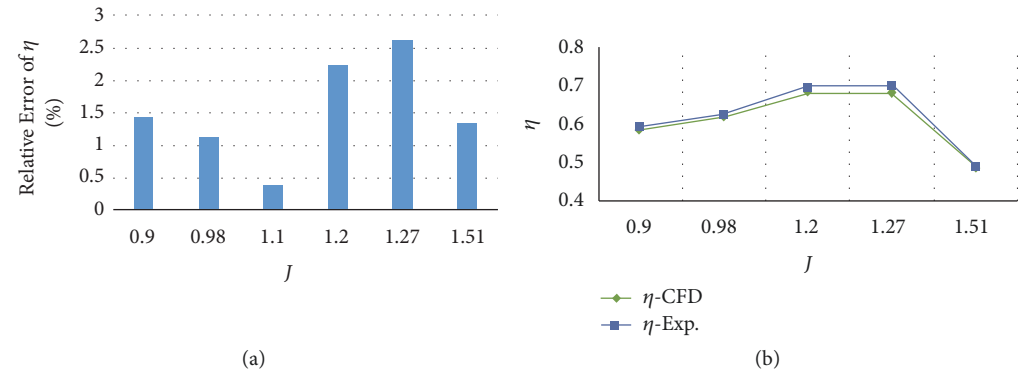

FIGURE 6: (a) A relative error diagram of simulated results of propeller efficiency η; (b) hydrodynamic performance prediction and test curve of η.

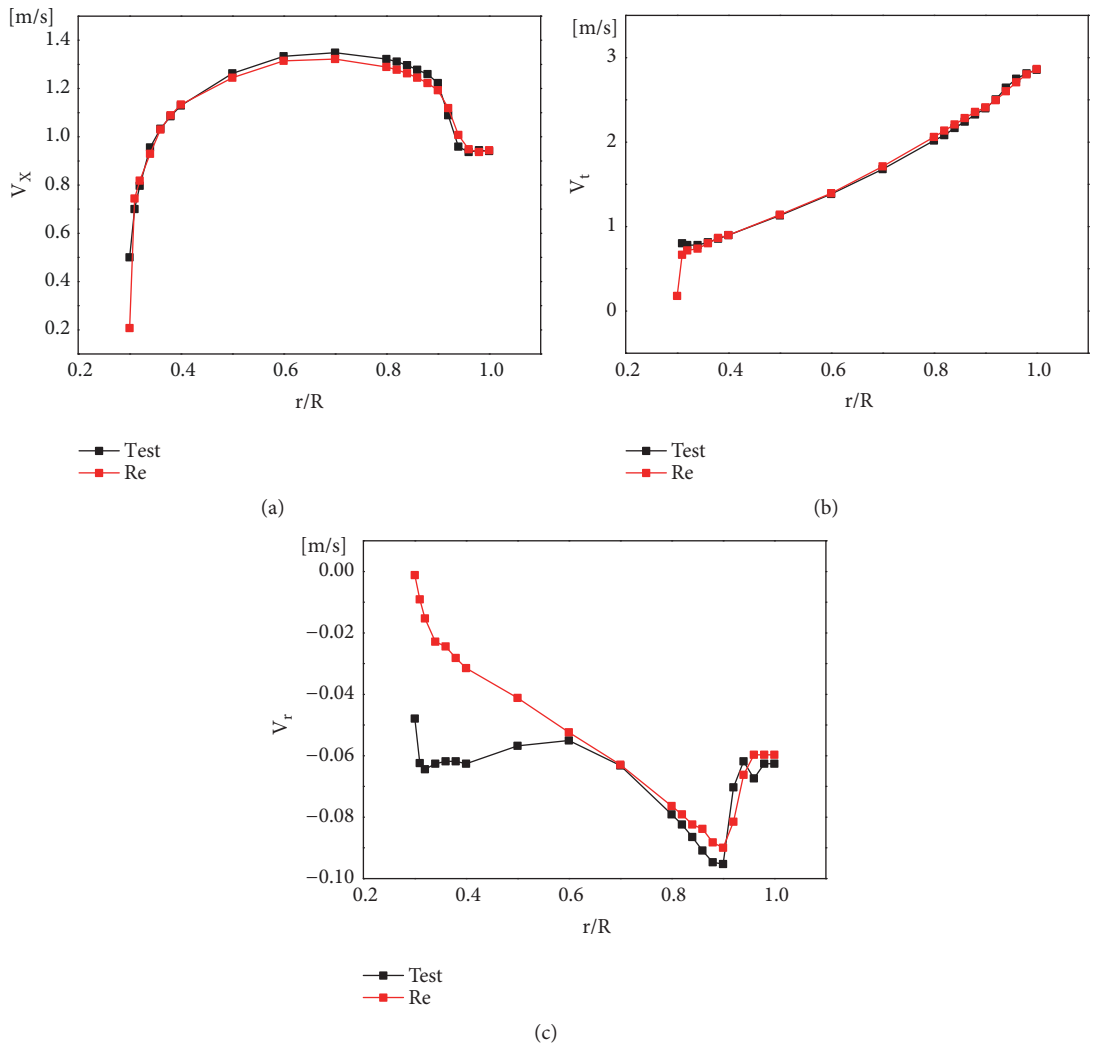

FIGURE 7: Distributions of three velocity components on a particular plane of x/R= 0.2386. (a) Axial velocity components (V_x); (b) tangential velocity components (V_t); (c) radial velocity components (V_r).

J=1.1, respectively, which were twice over than this paper. Hence the new model obtained more accurate performance prediction compared with some published literatures (for example, and as a contrast, Sun [7], Morgut et al. [8, 9], Zhao [10], and Tong [22]). Even through the errors of K_t and K_q in Yang's work were slightly smaller than ours [23], their propeller efficiency η was much larger than this paper.

The experimental results of axial, tangential, and radial velocity components at different radial distances r of the propeller downstream x/R=0.2386 were compared with the simulation results based on the standard k-ε model. The performance prediction ability of the new model was verified. x is the axial distance, and R is the propeller radius. Figure 7 is the distribution of axial (V_x), tangential (V_t), and radial (V_r) velocity components with dimensionless radial coordinates r/R, respectively. The experimental data of the three components are very close to the simulation results. The errors of axial and tangential velocity components are less than 3% when r/R is not less than 0.34. Because of the small longitudinal coordinates of the radial component, it can be clearly found that the simulation results are closer to the experimental results when the r/R was not less than 0.6. In addition, the radial component is close to zero when the radial component is less than 0.6 this is because the model is simplified and the radial velocity of the axis surface is zero.

4. Results and Discussion

4.1. Blade Pressure. The accurate prediction of the pressure distribution on the propeller blade was important for analyzing the flow characteristics of a propeller design. When the turbulence was fully developed on blade surfaces, the pressure gradient was expected to be nearly similar with different advance coefficients (J). The pressure side distribution predicted in the transition simulation (Figure 8) showed a strong pressure gradient along the tangential direction near the leading edge region. Under low advance coefficients, the pressure distribution on blade pressure side varied greatly,

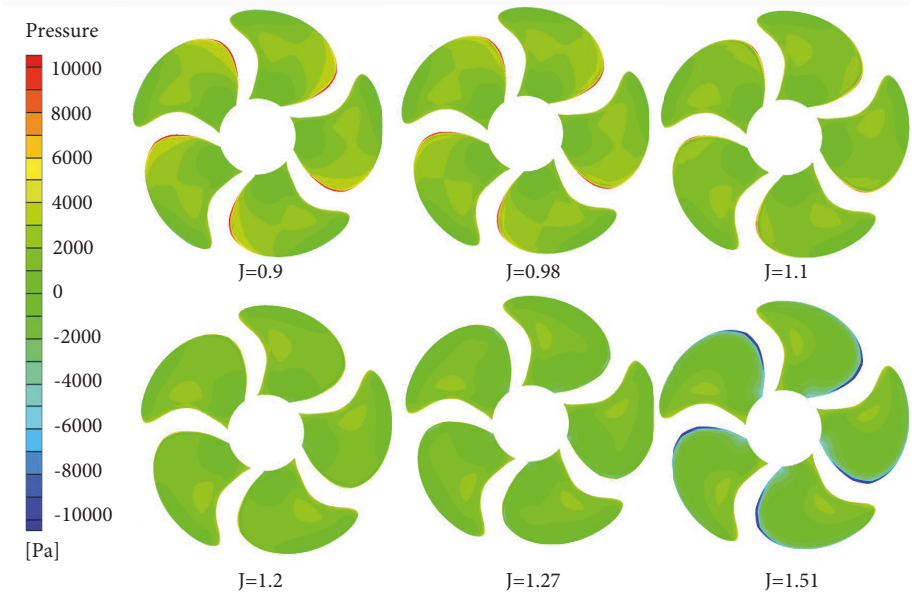

Figure 8: Pressure profile on the pressure side.

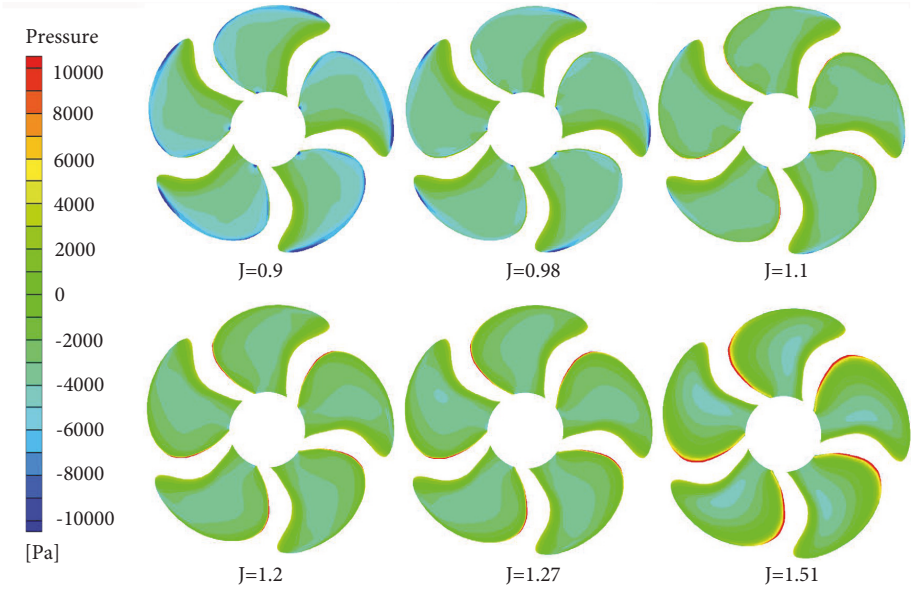

Figure 9: Pressure profile on the suction side.

and the nonuniformity of flow field was more obvious. The negative pressure on the leading edge aroused due to the negative incidence angle with the increase of J. On the contrary, the evident change had not been found on the other region.

Focusing on the pressure on the suction side shown in Figure 9, the pressure gradient was complicated because the velocity of the uniform free-stream flow got larger. There were two regions with the low value of pressure and strong pressure gradient at lower load (J=0.9, 0.98), which were the blade tip region and the blade root near the leading edge, respectively. However, the conspicuous region disappeared, owing to the pressure got larger with the increase of J. The region near the leading edge provided a larger value of pressure when the advance coefficient was a larger value (J=1.2, 1.27, 1.51). The pressure changed largely with the advance coefficient J, because the effect of advance velocity out weighted the spinning as the coefficient increased. As the increase of J, the thrust and torque decreased rapidly with the decrease of the incidence angle.

4.2. Velocity Profile and Streamlines. In Figure 10 the profiles of computed velocity magnitude field were presented. The large velocity gradients in the tip region were shown. It could be seen that the flow was concentrated between the blades

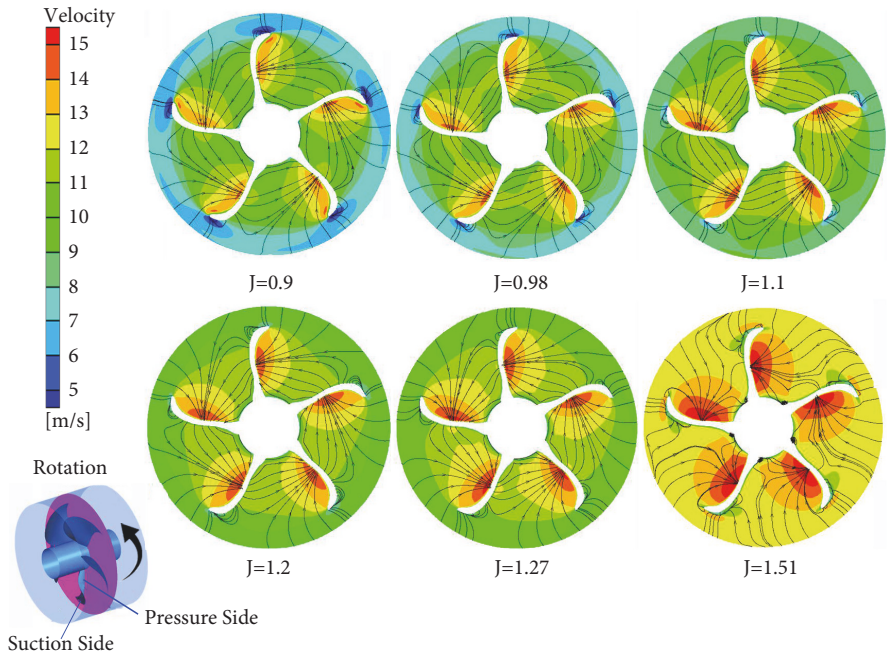

Figure 10: Velocity and streamlines profile on the plane of x=0.

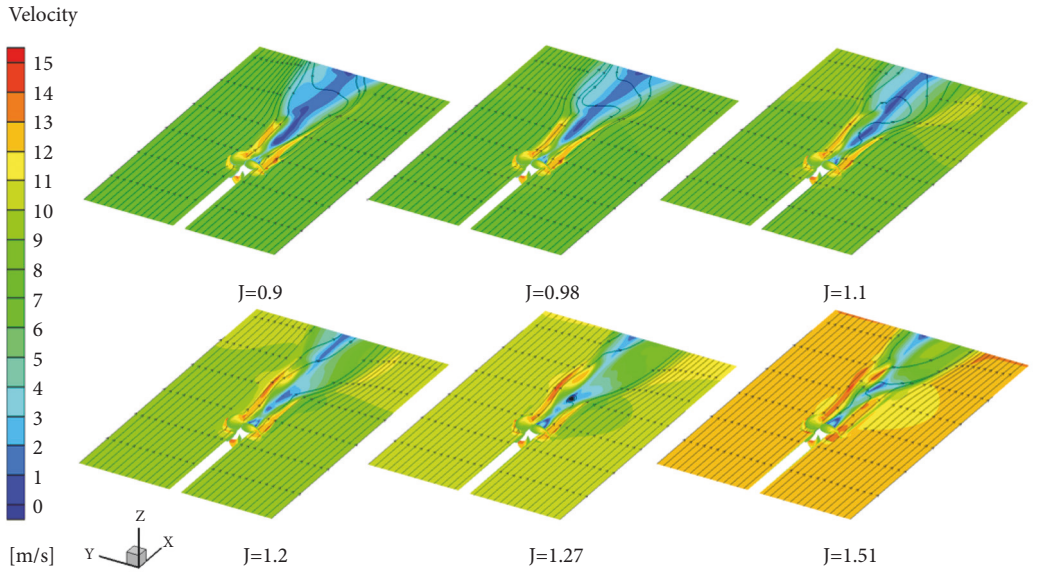

Figure 11: Velocity field on the plane of z=0.

of the propeller, and the maximum velocity occurred in the middle of the blade. Because of the rapid flow at the tip of the blade, there was a pressure difference on both sides of the blade, where the flow separation occurred, resulting in the formation of tip vortices. It was note that those streamlines, starting in the pressure side and ending in the suction side, described the flow direction between blades. When moving between the blades, the fluid absorbed the energy of the propeller and its kinetic energy increased. Subsequently, the tip vortices weakened due to the fact that the propeller was gradually unloaded with the increase of J. The effect of the increase of incoming flow velocity on the flow field was obvious.

Figure 11 showed the velocity field in the plane of z=0. The near field behind the blade was dominated by the blade trailing edge wake, where the streamlines were nearly parallel with the x-axis. These streamlines became unstable and eventually twisted up to form the far wake. Meanwhile, the

area behind the propeller hub was always full of curving and tortuous streamlines, which had some important impact on that field behind the blade to make the streamlines more unstable. With the increase of J, the load of propeller disk decreased at a higher rate, which could be proved by the stronger and wider high regions of velocity contours. Moreover, the phenomenon of the marked asymmetric distribution of velocity profiles was probably caused by the strong interaction between the tip and hub vortices and the possible triggering of the hub instability during wake convection.

It was interesting to note that the middle area closing to the outlet boundary provided a lower velocity, where the streamlines twisted up clearly but the backflow did not appear, which indicated that the computational domain with the fat cylinder was applicable to obtain the highly accurate predicted results. In conclusion, the velocity flow not only explained the reason why the blade and streamlines changed with the advance coefficient but also suggested that the computational domain was rational.

5. Conclusion

In this paper, the propeller DTMB P5168 was chosen to carry out the investigation. The purpose of this study was to improve the performance prediction ability of marine propellers under steady flow. Owing to employ the Multiple Reference Frame (MRF) approach, the computational domain was subdivided into *Rotating* and *Fixed* parts. In this paper, propeller performance parameters were measured and simulated in steady conditions, such as the velocity field on the propeller plane and so forth. The results obtained by the two methods are identical. Some conclusions had been drawn.

Except for the case of J=1.51, on different advance coefficients J, the errors of K_t and K_q were less than 5% and 3%, respectively. However, no matter what value J took, the error of η was less than 2.62%. Compared with some previous research results, the fat passage model achieved more accurate performance prediction. The circumferentially averaged velocity components were also compared with the experimental values. The axial and tangential velocity components were also in good agreement with the experimental data. The radial velocity had the same trends as the experimental data at the large value of J.

With the increase of J, the pressure near the leading edge reduced rapidly on the pressure side and increased on the suction side, which resulted in the fact that the thrust lessened remarkably. It could be seen that, on the plane of x=0, the streamlines started in the pressure side and ended in the suction side. Besides, the tip vortices weakened due to the gradual unloading of the propeller with the increase of J. The velocity field in the plane of z=0 showed that the middle area closing to the outlet boundary provided a lower velocity, where the streamlines twisted up clearly without the appearance of backflow, which indicated that the computational domain was a correct and logical choice.

Despite lacks of computation capacity, the steady-state simulation with hexastructured girds still provides a detailed understanding of the potential physical phenomena. CFD is a useful tool to validate and improve the performances of marine propeller models, which can play an important role in shortening the design cycle.

Nomenclature

D: Propeller diameter, 0.4027 m
R: Propeller radius, m
n: Propeller rotational speed, rev/s
V: Incoming flow velocity, m/s
J: Advance coefficient, $V/(n{\cdot}D)$
Q: Torque, N
T: Thrust, N·m
K_q: Torque coefficient, $Q/(\rho{\cdot}n^2{\cdot}D^5)$
K_t: Thrust coefficient, $T/(\rho{\cdot}n^2{\cdot}D^4)$
η: Propeller efficiency, $JK_T/(2\pi{\cdot}K_Q)$
V_x: Axial velocity, normalized by V, m/s
V_r: Radial velocity, normalized by V, m/s
V_t: Tangential velocity in the rotating frame, normalized by V, m/s
x: Axial coordinate, from propeller mid plane
ρ: Density, 998 kg/m^3
ν: Kinematic viscosity, m^2/s.

Data Availability

The data used to support the findings of this study are available from the corresponding author upon request.

Conflicts of Interest

The authors declared that there were no conflicts of interest regarding the publication of this paper.

Acknowledgments

This work was supported by the Postdoctoral Fund of Liaoning Province (Grant no. 20170520351), the Key Scientific and Technological Projects of Jilin Province (Grant no. 20170204066GX) and Science and Technology Projects of the Edcation Department of Jilin Province (Grant No. JJKH20180137KJ).

References

[1] E. G. Paterson, R. V. Wilson, and F. Stern, "General-purpose parallel unsteady RANs ship hydrodynamics code: CFDSHIP-Iowa," Defense Technical Information Center, 2003.

[2] T. Watanabe, T. Kawamura, Y. Takekoshi, M. Maeda, and S. Hyung, "Simulation of steady and unsteady cavitation on a marine propeller using a RANS CFD code," in *Proceedings of the 5th International Symposium on Cavitation*, Osaka, Japan, 2003.

[3] F. D. Felice, M. Felli, M. Liefvendahl, and U. Svennberg, "Numerical and experimental analysis of the wake behavior of a generic submarine propeller," *Prism*, vol. 1, no. 8, p. 158, 2009.

[4] J. Yao, "Investigation on hydrodynamic performance of a marine propeller in oblique flow by RANS computations," *International Journal of Naval Architecture and Ocean Engineering*, vol. 7, no. 1, pp. 56–69, 2015.

[5] L. Wang, C. Guo, Y. Su, P. Xu, and T. Wu, "Numerical analysis of a propeller during heave motion in cavitating flow," *Applied Ocean Research*, vol. 66, pp. 131–145, 2017.

[6] M. R. Naseer, E. Uddin, K. Rana, and S. Zahir, "Computational validation of hydrodynamic and hydroacoustic performance of marine propeller," in *Proceedings of the 14th International Bhurban Conference on Applied Sciences and Technology, IBCAST 2017*, Pakistan, January 2017.

[7] S. Joseph, "Two-phase Eulerian averaged formulation of entropy production for cavitation flow," University of Manitoba, 2014.

[8] M. Morgut and E. Nobile, "Comparison of hexa-structured and hybrid-unstructured meshing approaches for numerical prediction of the flow around marine propellers," in *Proceedings of The First International Symposium on Marine Propulsors*, Trondheim, Norway, 2009.

[9] M. Morgut and E. Nobile, "Influence of grid type and turbulence model on the numerical prediction of the flow around marine propellers working in uniform inflow," *Ocean Engineering*, vol. 42, pp. 26–34, 2012.

[10] Q. Zhao, *Towards Improvement of Numerical Accuracy for Unstructured Grid Flow Solver*, University of Toledo, USA, 2012.

[11] X. Wang and K. Walters, "Computational analysis of marine-propeller performance using transition-sensitive turbulence modeling," *Journal of Fluids Engineering*, vol. 134, no. 7, p. 071107, 2012.

[12] G. Dubbioso, R. Muscari, F. Ortolani, and A. Di Mascio, "Analysis of propeller bearing loads by CFD. Part I: Straight ahead and steady turning maneuvers," *Ocean Engineering*, vol. 130, pp. 241–259, 2017.

[13] G. Dubbioso, R. Muscari, and A. Di Mascio, "Analysis of the performances of a marine propeller operating in oblique flow," *Computers & Fluids*, vol. 75, pp. 86–102, 2013.

[14] G. Dubbioso, R. Muscari, and A. Di Mascio, "Analysis of a marine propeller operating in oblique flow. Part 2: Very high incidence angles," *Computers & Fluids*, vol. 92, pp. 56–81, 2014.

[15] C. Yu, Y. Wang, C. Huang, X. Wu, and T. Du, "Large eddy simulation of unsteady cavitating flow around a highly skewed propeller in nonuniform wake," *Journal of Fluids Engineering*, vol. 139, no. 4, p. 041302, 2017.

[16] A. Di Mascio, R. Muscari, and G. Dubbioso, "On the wake dynamics of a propeller operating in drift," *Journal of Fluid Mechanics*, vol. 754, pp. 263–307, 2014.

[17] N. Chase and P. M. Carrica, "Submarine propeller computations and application to self-propulsion of DARPA Suboff," *Ocean Engineering*, vol. 60, pp. 68–80, 2013.

[18] ANSYS® Academic Research, *Help System*, ANSYS, Inc., 1st edition edition, 2015.

[19] B. E. Launder and D. B. Spalding, *Lectures in Mathematical Models of Turbulence*, 1972.

[20] C. Chesnakas and S. Jessup, "Experimental characterization of propeller tip flow," in *Proceedings of the 22nd Symposium on Naval Hydrodynamics*, Washington, USA, 1998.

[21] N. E. Gharbi, R. Absi, A. Benzaoui, and E. H. Amara, "Effect of near-wall treatments on airflow simulations," in *Proceedings of the 2009 International Conference on Computational Methods for Energy Engineering and Environment*, pp. 185–189, Tunisia, 2009.

[22] T. Bo et al., "Numerical prediction for the hydrodynamic performance of a ferry propeller," *Chinese Journal of Ship Research*, vol. 9, no. 1, pp. 52–58, 2014.

[23] Q. F. Yang, Y. S. Wang, and Z. H. Zhang, "Effects of non-uniform inflow on propeller cavitation hydrodynamics," *Chinese Journal of Hydrodynamics*, vol. 26, no. 5, pp. 538–550, 2011.